1.1-μm-waveband tunable laser using emission-wavelength-controlled InAs quantum dots for swept-source optical coherence tomography applications

Toshiya Tsuji[1], Nobuhiko Ozaki[1,*], Sho Yamauchi[1], Katsuya Onoue[1], Eiichiro Watanabe[2], Hirotaka Ohsato[2], Naoki Ikeda[2], Yoshimasa Sugimoto[2], David T. D. Childs[3], and Richard A. Hogg[3]

[1]*Faculty of Systems Engineering, Wakayama Univ., Wakayama 640-8510, Japan*

[2] *National institute for materials science, Tsukuba, Ibaraki 305-0047, Japan*

[3] *James Watt School of Engineering, University of Glasgow, Glasgow, G12 8LT, U.K.*

*E-mail: ozaki@wakayama-u.ac.jp

In this study, an optical gain chip using emission-wavelength-controlled self-assembled InAs quantum dots (QDs) was developed for swept-source optical coherence tomography (SS-OCT) applications. The optical characterizations indicated that the QDs emission wavelength and optical gain spectra were controlled in the 1.1-μm-waveband by optimizing the QDs growth conditions. This waveband is useful for obtaining a large imaging depth of OCT because of an optimal balance between absorption and scattering in biological samples. In addition, continuous tunable lasing in the waveband was achieved by introducing the QD-based gain chip into a grating-coupled external cavity. This tunable laser was introduced into a SS-OCT setup, and the point-spread function (PSF) was evaluated. The PSF position was observed to vary according to the optical path length differences. These results demonstrate the feasibility of the application of emission-wavelength-controlled QDs for SS-OCT.

1. Introduction

Near-infrared (NIR) light is widely used in various applications such as medical imaging technology. For instance, optical coherence tomography (OCT)[1)], which is a non-invasive profile imaging technology, has been developed by utilizing NIR broadband light sources. OCT is based on low-coherence interferometry; thus, broadband light sources have been utilized to obtain OCT images of which the axial resolution is inversely proportional to the bandwidth of the light source[2)]. Recently, OCT has been developed to obtain a relatively long imaging depth by using a tunable laser as the broadband swept light source, known as the swept-source (SS)-OCT[3)]. The axial resolution of SS-OCT depends on the tunable range of the laser; thus, a widely tunable laser is required for SS-OCT. In addition, the waveband of the light source should preferably be within the NIR wavelength because a large penetration depth can be obtained in biological samples owing to the low absorption coefficient[4)]. In particular, a 1.0–1.1-μm wavelength band provides an optimal balance between absorption and scattering in biological tissues.

Thus, the development of broadband tunable lasers in the 1.1-μm-waveband for SS-OCT applications has been required. Semiconductor-based tunable lasers have proven to be suitable because they serve as compact, robust, and cost-effective light source devices. However, it is difficult to obtain a wide range of tunable lasing using conventional semiconductor materials, such as quantum wells. In contrast, self-assembled InAs quantum dots (QDs)[5)] are ideal broadband optical gain materials. As an ensemble of InAs QDs has an inherent size and In composition distributions, a broadband emission and gain spectra in the NIR regions, typically in the 1.2–1.3-μm range, can be easily obtained[6–12)]. Many studies have demonstrated the development of broadband tunable lasers based on self-assembled InAs QDs[13–22)]. In addition to the broadband emission and gain properties, we focused on the emission wavelength controllability of InAs QDs through optimization of the growth conditions[23–28)]. In this study, we altered the emission wavelength of the QDs from the typical emission center wavelength of InAs QDs grown on GaAs at 1.2-μm to the 1.1-μm-waveband. Subsequently, a QD-based tunable laser was developed using a grating-coupled external cavity (EC). Furthermore, we introduced a QD-based EC tunable laser in the SS-OCT setup and verified its suitability for SS-OCT applications. As mentioned above, a QD-based 1.2–1.3-μm-waveband tunable laser has been reported by several other research groups[13–22)]; however, the development of a 1.1-μm-waveband tunable laser based on emission-wavelength-controlled InAs QDs to demonstrate the feasibility of SS-OCT light source applications is considered to be a novel research work.

2. Experimental methods

2.1 QD-based gain chip fabrication

Figure 1(a) illustrates a schematic of the fabricated QD-based gain chip. First, a sample including four stacked layers of self-assembled InAs QDs was grown on a GaAs substrate via molecular beam epitaxy. The QDs were embedded in a 240-nm-thick GaAs waveguide layer, which was sandwiched between 1.5-μm-thick p-/n-$Al_{0.35}Ga_{0.65}As$ cladding layers for optical and electronic confinement. The InAs QDs were grown owing to the strain caused by the lattice mismatch between GaAs and InAs via the Stranski–Krastanov (S–K) growth mode[5]. The substrate temperature was set at approximately 480 °C, and InAs was deposited at a growth rate of 0.2 monolayer (ML)/s. The total amount of supplied InAs was approximately 2 ML. After the growth of each InAs QD layer, a GaAs layer (approximately 48 nm in thickness) was deposited to embed and space the QD layers. The growth conditions of this GaAs layer were optimized to control the emission wavelength of the embedded InAs QDs. During the growth of the GaAs layer, the substrate temperature was decreased to approximately 450 °C, which is slightly higher (by 20–30 °C) than that for normal InAs QDs emitting at longer (1.2–1.3-μm) wavelength. In addition, the growth interruption time to ripen QDs after the InAs supply was omitted, whereas a growth interruption time of approximately 30 s was provided for normal QDs. These variations in growth conditions may alter the QDs to be more soluble during the capping process because of the In atom migrations from QDs, which could result in size reduction and shortening of the emission wavelength of QDs[27,28].

Next, a straight ridge-type waveguide (RWG) with a width of 5 μm and height of 1.4 μm was fabricated on the QD-grown wafer using photolithography and dry-etching techniques. After deposition and area-selective wet-etching of a thin SiO_2 insulation film on the RWG, contact electrodes were formed on both sides of the wafer. The wafer was cleaved to form an edge-emitting chip of 2 × 2 mm^2.

2.2 Characterizations of lasing with the QD-based gain chip

As depicted in Fig. 1(b), the QD-based gain chip was placed on a stage with a thermoelectric cooler at a temperature of 25 °C. Continuous-wave currents were then applied to the gain chip, and edge-emitting electroluminescence (EL) spectra were measured using an optical spectrum analyzer through a lensed fiber. From the obtained EL spectra of the chip, the gain spectra of the fabricated chip were measured using the Hakki–

Paoli (H–P) method[29] under various injection currents. According to the H–P method, the modulation depth can be used as the gain parameter; the net modal gain (Gi) can be expressed by the formula:

$$G_i = \frac{1}{L}\ln\left(\frac{\sqrt{\gamma_i}-1}{\sqrt{\gamma_i}+1}\right) + \frac{1}{L}\ln\left(\frac{1}{R}\right),$$

where L is the cavity length, γ_i is the ratio of the peak and valley intensities, and R is the reflectivity at the edge of the cavity.

A grating-coupled EC was employed to obtain a tunable laser from the QD-based gain chip. A blazed diffraction grating (1200 grooves/mm) was used for optical feedback with continuously varying wavelengths through the other side of the gain chip.

2.3 SS-OCT setup

Subsequently, the QD-based EC tunable laser was introduced into the SS-OCT system (Fig. 1(c)). The tunable laser light was divided using a 50:50 coupler, and the two lights reflected from the reference and sample mirrors were interfered through the coupler. The interference signal was detected using the photodetector as a signal intensity oscillating in the time domain with a beat frequency depending on the optical path difference (d) between the two mirrors. Then, the point spread function (PSF) was obtained by the inverse Fourier transformation of the signal, representing the spatial reflectivity along the axial direction[30]. We obtained PSFs for the sample mirror set at various positions in the axial direction to verify the setup available for SS-OCT applications.

3. Results and discussion

3.1 Characterization of the QD-based gain chip

Figure 2(a) depicts the photoluminescence (PL) spectra obtained from the fabricated QD-based gain chip (red solid line) and typical InAs QDs grown under normal growth conditions as a reference (black dashed line). Both spectra exhibit a broad emission line with a peak that can be attributed to carrier recombination between the ground states (GS) of the QDs. The PL obtained from the QDs in the fabricated chip exhibited a GS peak wavelength of approximately 1150 nm, which was blue-shifted by approximately 65 nm from that of normal QDs. The linewidth of the GS emission peak was slightly increased (approximately 45 meV) compared to that of normal QDs (approximately 34 meV). These results demonstrate the successful emission wavelength control of QDs to the 1.1-μm waveband through the optimization of the growth conditions. Although further investigation is

necessary, the modified growth conditions of the capping process possibly enhance the In atom migration from QDs, resulting in a reduction in the mean size and an increase in the distribution of size and In composition. This could cause a blue-shift in the emission peak wavelength and broadening of the linewidth.

From the EL measurements, the fabricated QD-based gain chip was confirmed to exhibit Fabry–Perot (F–P) lasing beyond the threshold injection current, which was estimated to be 65 mA from the *L–I* curve depicted in Fig. 2(b). A typical F–P lasing spectrum under an injection current of 100 mA is shown in the inset of Fig. 2(b). Considering that several mW output power (through the lensed fiber) was achievable from the chip even with as-cleaved edges (without any coatings) and only four stacked QD layers, the luminous efficiency of the fabricated chip is comparable with that of conventional QD-based LDs, and the fabricated chip can be used as an optical gain medium for a tunable laser light source. To investigate the optical gain property of the chip, the gain spectra were deduced by the H–P method. As depicted in Fig. 3(a), a high-resolution (nominal resolution value of 0.02 nm) EL spectrum exhibits modulation with the free spectral range, corresponding to the F–P longitudinal modes that are expected to be approximately 0.1 nm. Fig. 3(b) depicts the gain spectra evaluated from the peaks and valleys of the spectrum under various injection currents (60–64 mA) below the threshold current. The gain peak wavelength was approximately 1146 nm, which corresponded well with the F–P lasing wavelength (1147 nm) shown in the inset of Fig. 2(b). The gain bandwidth was gradually increased up to approximately 70 nm with an increase in the injection current. From these results, the QD-based gain chip can be expected to provide tunable lasing in the injection currents under the threshold current of the internal F–P lasing.

3.2 Tunable lasing

The QD-based gain chip was installed into the grating-coupled EC, as illustrated in Fig. 1(b). By rotating the brazed diffraction grating on the quasi-Littrow configuration, the wavelength of the reflected light is varied and tunable lasing can be performed. Figure 4(a) shows the tunable lasing spectra obtained under various injection currents. Clearly, continuous variations in the laser emission wavelength were obtained in the 1.1-μm waveband, and the tunable range was increased with in the injection current up to 17 nm at 64 mA. Although the tunable ranges were smaller than the optical gain ranges estimated by the H–P method, the tunable lasing behaviors were confirmed from the QD-based gain chip. The tuning range of the external cavity is dependent on the internal loss in the gain

chip and external losses, including the coupling losses between the chip and external cavity, whereas the gain spectrum obtained from the H–P method is only dependent on the internal optical loss in the gain chip. As a result, the external tuning range could be less than the bandwidth of the chip gain. Additional measures to reduce the external losses, for instance, an anti-reflection coating of the chip edge coupled to the external cavity and the use of a high-reflectance grating, should be effective in extending the tuning range.

The linewidth and dynamic range of a single lasing peak at a fixed grating position were approximately 0.23 nm and 34 dB, respectively, as depicted in the right of the bottom row of Fig. 4(a). In addition, the dynamic range variation with the lasing wavelength was measured, as shown in Fig. 4 (b). This could be related to the gain variation of the QD gain chip. To confirm this relationship, the threshold current of each EC laser wavelength was measured, as indicated by the black solid line in Fig. 4(c). The threshold current is inversely proportional to the gain spectrum; thus, the lowest current in the solid line curve corresponded to the peak wavelength of the dynamic range shown in Fig. 4(b). The tunable ranges of the EC laser under various injection currents are consistently within the solid line curve. The tunable range values were defined between the minimum and maximum wavelengths, where the decrease in the laser intensities was less than -6dB from the maximum laser intensity. These results demonstrate the EC tunable lasing using the QD-based gain chip.

When this tunable laser is introduced into the SS-OCT, the optical axis resolution (Δz) and the coherence length (Δl_c) can be estimated to be 35 μm and 1.26 mm, respectively, from the approximate formulae:

$$\Delta z = \frac{2ln2}{\pi}\frac{\lambda_0^2}{\Delta\lambda}, \Delta l_c = \frac{ln2}{\pi}\frac{\lambda_0^2}{\delta\lambda} .$$

Although these values are not comparable with the state-of-the-art SS-OCT, further measures such as anti-reflection coating of the gain chip and use of high reflectance grating should improve these values.

3.3 Evaluation of QD-based tunable laser as a light source of SS-OCT

Finally, the QD-based tunable laser was installed in the SS-OCT system to evaluate the tunable laser as a SS-OCT light source. Using SS-OCT with the QD-based tunable laser, interference signal intensities with various values of d (0.2–1.0 mm) were obtained, as shown in Fig. 5(a). These signals oscillated with the beat frequency in accordance with the value of d. The inverse Fourier transformed spectra indicate the PSFs with different d values, as shown in Fig. 5(b). The peak positions of the PSF corresponded well with the

actual *d* values. Although the interference signal was modulated in non-sinusoidal waveforms, which could be attributed to the anisotropic reflection of the blazed grating, the Fourier-transformed peak position provided a reasonable value for the sample position. These results demonstrate the operation of low-coherence interferometry using the SS-OCT system.

The PSFs obtained with various *d* values were arranged on the same scale, as shown in Fig. 5(c). The red line represents the fitting of the first five peaks. The decay of the peak intensity, which is known as the sensitivity roll-off, was estimated to be -5.2 dB/mm. The coherence length, defined as the length required for reducing the peak intensity at -6 dB, was approximately 1.15 mm, which corresponded well with the value estimated from the laser linewidth (1.26 mm). For the latter five PSF peaks, the decay ratio was estimated to be -8.5 dB/mm. This reduction in the decay rate could be attributed to the lower coupling efficiency of the reflected light into the optical fiber. From these results, reasonable SS-OCT operations using a QD-based tunable laser were demonstrated.

4. Conclusions

A tunable laser with an emission range of 1.0–1.1 μm was developed using emission-wavelength-controlled QDs. The emission and optical gain spectra of the QDs were successfully controlled in the waveband by optimizing the growth conditions. In addition, continuous laser tuning with a grating-coupled EC was confirmed. By using the QD-based tunable laser, reasonable SS-OCT operations were demonstrated. In this study, the QD-based gain chip was used under the threshold current of internal F–P lasing. Thus, a further extension of the tunable range can be expected by suppressing the internal lasing of the chip using an anti-reflection coating or bending RWG fabrication, resulting in a broader gain spectrum of the QDs under higher injection currents.

Acknowledgments

This work was partly supported by JSPS KAKENHI (Grant Numbers 16H03858, 16KK0130, and 20H02183) and the Consortium of Higher Education Institutions in Wakayama. The QD gain chip fabrications were supported by the NIMS Nanofabrication Platform in the “Nanotechnology Platform Project” sponsored by the Ministry of Education, Culture, Sports, Science and Technology (MEXT), Japan.

References

1) D. Huang, E. A. Swanson, C. P. Lin, J. S. Schuman, W. G. Stinson, W. Chang, M. R. Hee, T. Flotte, K. Gregory, C. A. Puliafito, J.G. Fujimoto, Science **254**, 1178 (1991).
2) M. E. Brezinski, *Optical Coherence Tomography: Principles and Applications* (Academic Press, New York, 2006).
3) W. Drexler and J. G. Fujimoto, *Optical Coherence Tomography: Technology and Applications* (Springer, Berlin, 2008).
4) M. S. Patterson, B. C. Wilson, D. R. Wyman, Lasers in Med. Sci. **6**, 379 (1991).
5) L. Goldstein, F. Glas, J. Y. Marzin, M. N. Charasse, G. Le Roux, Appl. Phys. Lett. **47**, 1099 (1985).
6) Z. Y. Zhang, R. A. Hogg, X. Q. Lv, and Z. G. Wang, Adv. Opt. Photonics **2**, 201 (2010).
7) M. Tsuda, T. Inoue, T. Kita, and O. Wada, Phys. Status Solidi C **8**, 331 (2011).
8) N. Ozaki, T. Yasuda, S. Ohkouchi, E. Watanabe, N. Ikeda, Y. Sugimoto, R. A. Hogg, Jpn. J. Appl. Phys. **53**, 04EG10 (2014).
9) S. Chen, W. Li, Z. Zhang, D. Childs, K. Zhou, J. Orchard, K. Kennedy, M. Hugues, E. Clarke, I. Ross, O. Wada, R. Hogg, Nanoscale Res. Lett. **10**, 340 (2015).
10) T. Yasuda, N. Ozaki, H. Shibata, S. Ohkouchi, N. Ikeda, H. Ohsato, E. Watanabe, Y. Sugimoto, and R. A. Hogg, IEICE Trans. Electron. **E99-C**, 381 (2016).
11) N. Ozaki, D. T. D. Childs, J. Sarma, T. S. Roberts, T. Yasuda, H. Shibata, H. Ohsato, E. Watanabe, N. Ikeda, Y. Sugimoto, and R. A. Hogg, J. Appl. Phys. **119**, 083107 (2016).
12) N. Ozaki, S. Yamauchi, Y. Hayashi, E. Watanabe, H. Ohsato, N. Ikeda, Y. Sugimoto, K. Furuki, Y. Oikawa, K. Miyaji, D.T.D. Childs, and R.A. Hogg, J. Phys. D: Appl. Phys. **52**, 225105 (2019).
13) H. Li, G. T. Liu, P. M. Varangis, T. C. Newell, A. Stintz, B. Fuchs, K. J. Malloy, and L. F. Lester, IEEE Photon. Technol. Lett. **12**, 759 (2000).
14) A. Kovsh, I. Krestnikov, D. Livshits, S. Mikhrin, and J. Weimert, Opt. Lett. 32, 793 (2007).
15) B. Stevens, D. Childs, K. Groom, M Hopkinson, R. Hogg, Appl. Phys. Lett. **91**, 121119 (2007).
16) X. Q. Lv, P. Jin, W. Y. Wang, and Z. G. Wang, Opt. Express **18**, 8916 (2010).
17) K. A. Fedorova, M. A. Cataluna, I. Krestnikov, D. Livshits, and E. U. Rafailov, Opt. Express **18**, 19438 (2010).
18) N. Yamamoto, K. Akahane, T. Kawanishi, H. Sotobayashi, Y. Yoshioka and H. Takai, Jpn. J. Appl. Phys. Lett. **51**, 02BG08 (2012).
19) G. Lin, P. Su, and H. Cheng, Opt. Express **20**, 3941 (2012).

20) S. Haggett, M. Krakowski, I. Montrosset, and M. A. Cataluna, Opt. Express **22**, 22854 (2014).
21) N. Ozaki, D. Childs, A. Boldin, D. Ikuno, K. Onoue, H. Ohsato, E. Watanabe, N. Ikeda, Y. Sugimoto, and R. Hogg, Proc. SPIE **10939**, 1093911 (2019).
22) T. Tsuji, N. Ozaki, S. Yamauchi, K. Onoue, E. Watanabe, H. Ohsato, N. Ikeda, Y. Sugimoto, D. T. D. Childs, and R. A. Hogg, Ext. Abstr. Solid State Devices and Materials, 2020, p. 315.
23) Y. Hino, N. Ozaki, S. Ohkouchi, N. Ikeda, and Y. Sugimoto, J. Cryst. Growth **378**, 501 (2013).
24) N. Ozaki, Y. Hino, S. Ohkouchi, N. Ikeda, and Y. Sugimoto, Phys. Status Solidi C **10**, 1361 (2013).
25) N. Ozaki, Y. Nakatani, S. Ohkouchi, N. Ikeda, Y. Sugimoto, K. Asakawa, E. Clark, R. A. Hogg, J. Cryst. Growth **378**, 553 (2013).
26) N. Ozaki, K. Takeuchi, Y. Hino, Y. Nakatani, T. Yasuda, S. Ohkouchi, E. Watanabe, H. Ohsato, N. Ikeda, Y. Sugimoto, E. Clarke, and R. A. Hogg, Nanomater. Nanotechnol. **4**, 26 (2014).
27) T. Kaizu, T. Matsumura, and T. Kita, J. Appl. Phys. **118**, 154301 (2015).
28) A. D. Utrilla, D. F. Grossi, D. F. Reyes, A. Gonzalo, V. Braza, T. Ben, D. González, A. Guzman, A. Hierro, P. M. Koenraad, J. M. Ulloa, Appl. Surf. Sci. **444**, 260 (2018).
29) B. W. Hakki and T. L. Paoli, J. Appl. Phys. **46**, 1299 (1975).
30) H. Shibata, N. Ozaki, T. Yasuda, S. Ohkouchi, N. Ikeda, H. Ohsato, E. Watanabe, Y. Sugimoto, K. Furuki, K. Miyaji, and R. A. Hogg, Jpn. J. Appl. Phys. **54**, 04DG07 (2015).

Figure Captions

Fig. 1. (a) Fabricated QD-based gain chip with straight RWG. (b) Setup for EL and grating-coupled EC tunable lasing measurements. (c) SS-OCT setup with the QD-based EC tunable laser.

Fig. 2. (a) EL spectra obtained from the fabricated QD-based gain chip under a low current (red solid line). The black dashed line represents the typical PL spectrum from InAs QDs. (b) *L-I* curve obtained from the fabricated QD-based gain chip.

Fig. 3. (a) High-resolution EL spectrum of the QD-based gain chip under an injection current of 64 mA; intensity oscillation due to the F–P cavity resonance was observed (inset). (b) Deduced optical gain spectra under various injection currents.

Fig. 4. (a) EL spectra obtained from the grating-coupled EC tunable laser with various injection currents. The lasing spectra were selected from continuous tuned laser spectra with an identical interval (approximately 0.5 nm). A single lasing peak at a fixed grating position under I = 64 mA is shown in the bottom right. (b) The dynamic range variation of the lasing peak as a function of the wavelength. (c) Threshold current plotted as a function of EC laser wavelength (black solid line) and the tunable range for various injection currents (red arrows).

Fig. 5. (a) Interference signals as a function of time with various optical path differences. (b) PSF variation with the optical path difference. (c) The analysis of the decay rate of the PSF intensity.

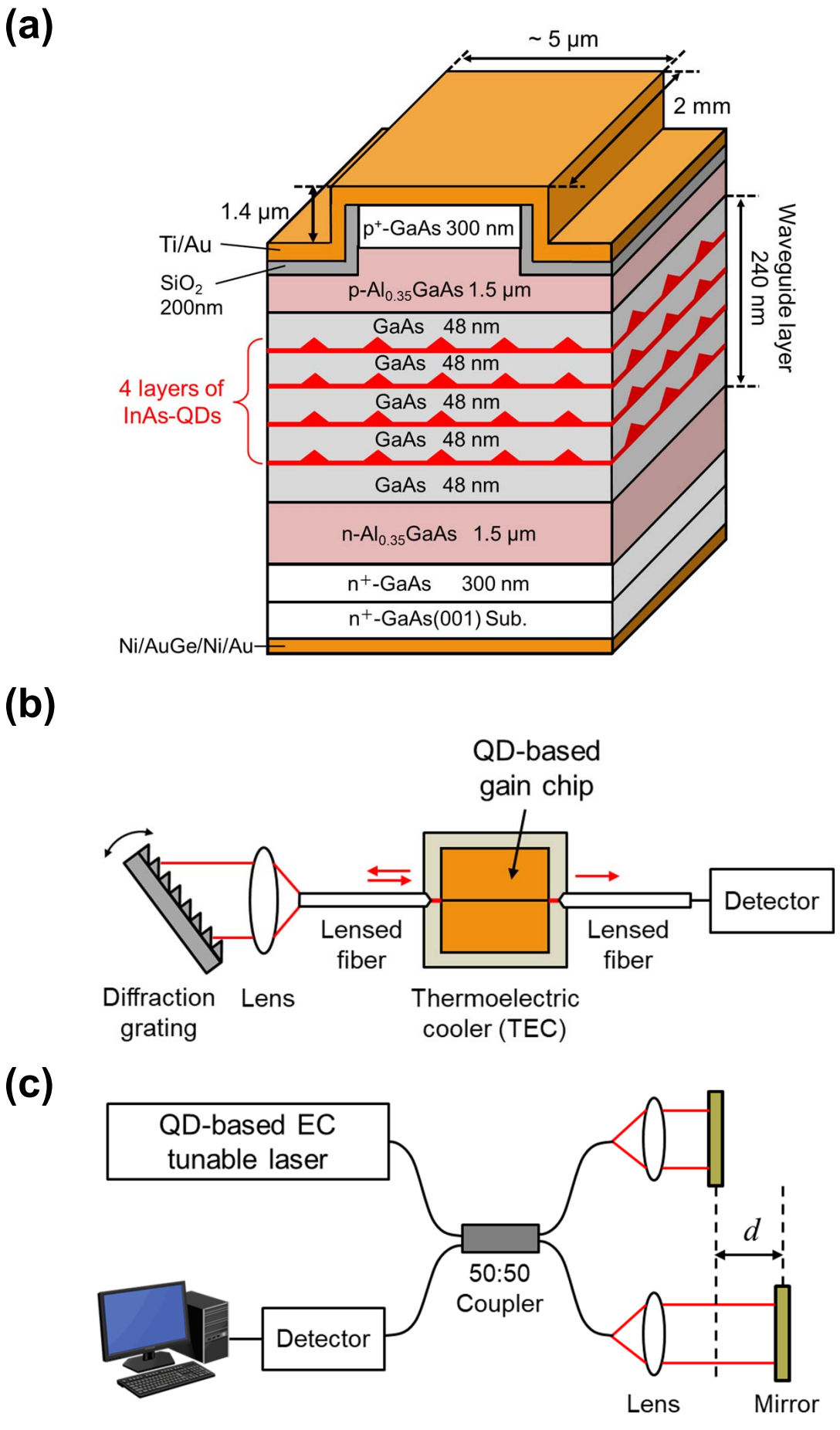

Fig. 1 T. Tsuji et al.

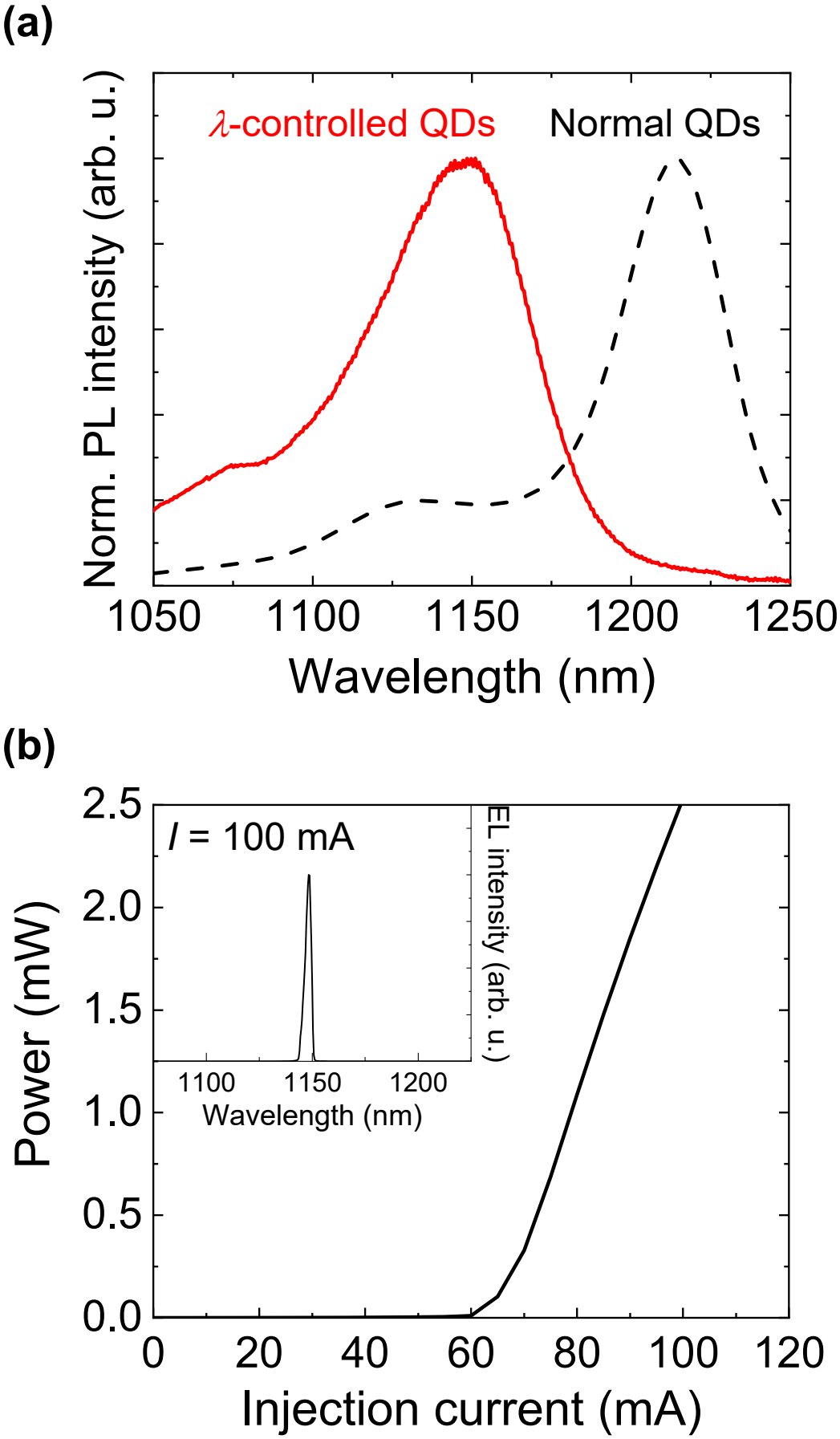

Fig. 2 T. Tsuji et al.

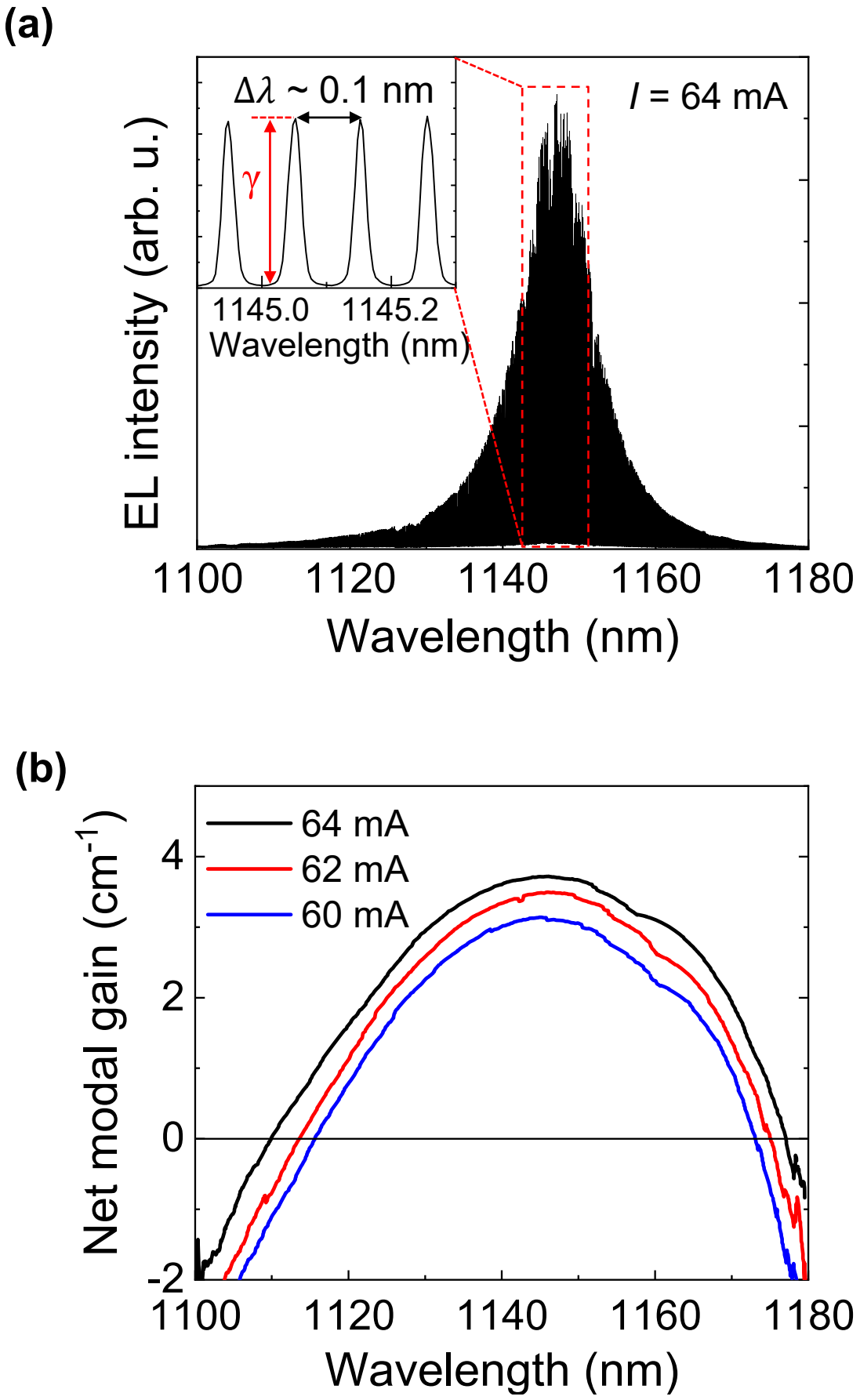

Fig. 3 T. Tsuji et al.

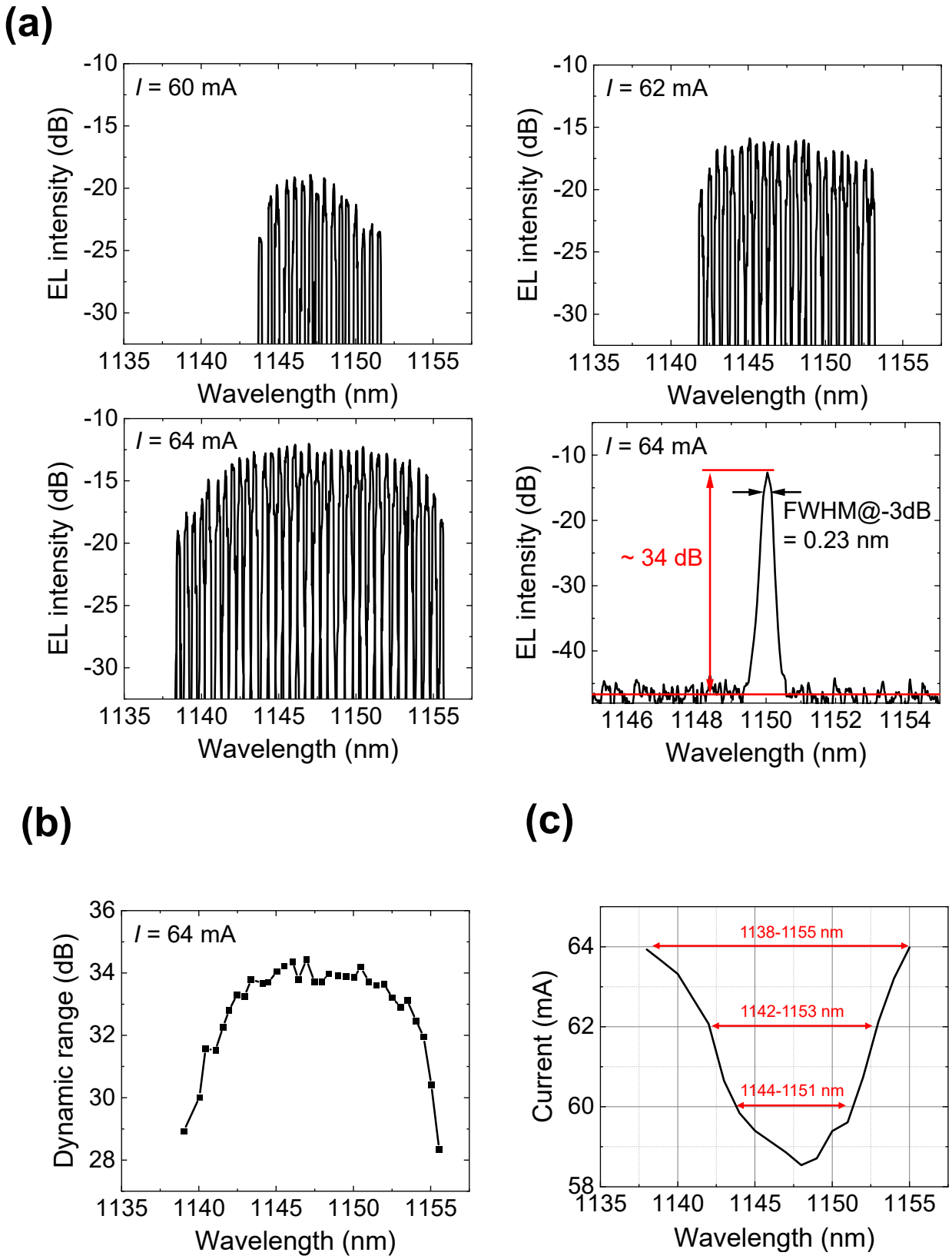

Fig. 4 T. Tsuji et al.

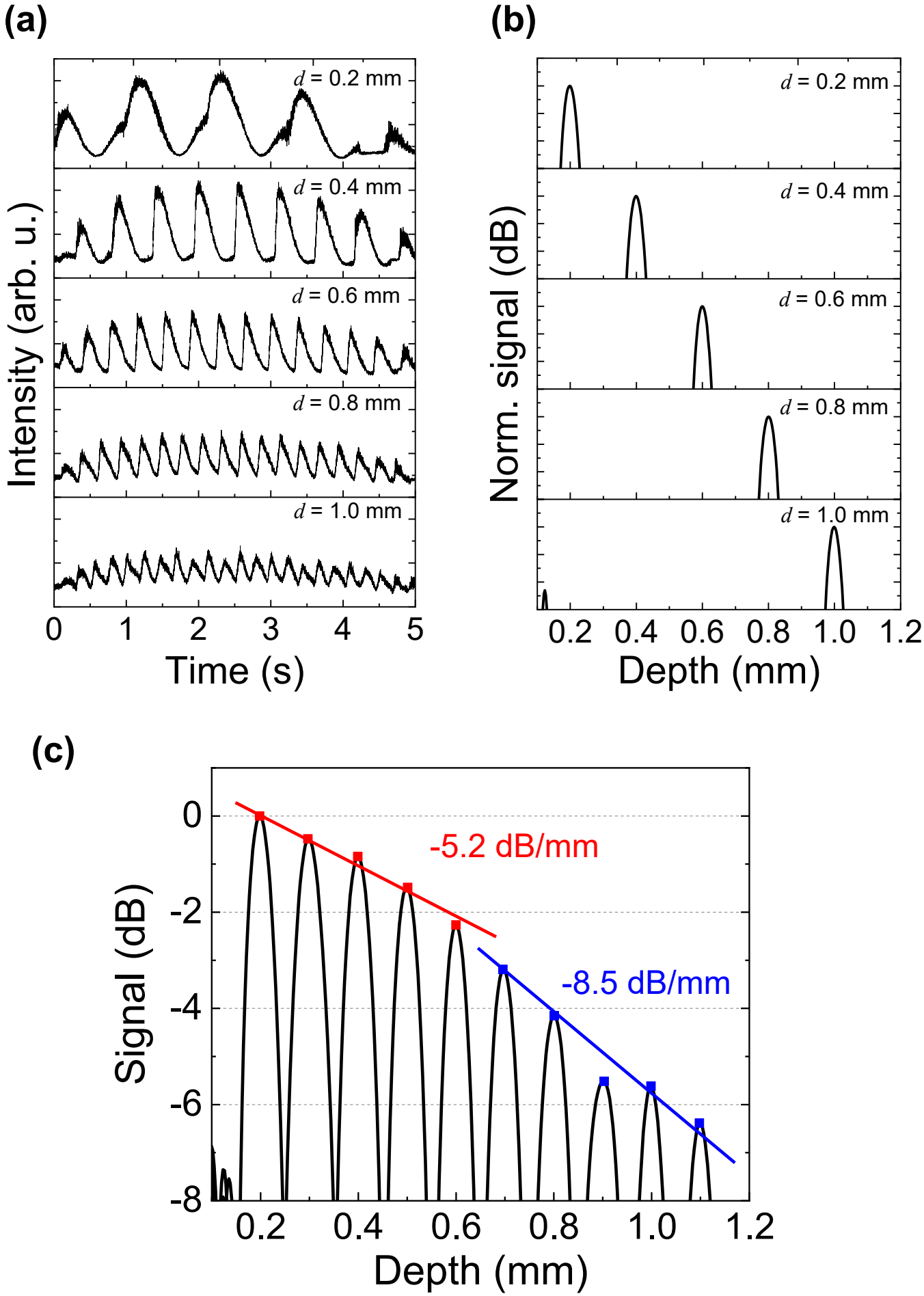

Fig. 5 T. Tsuji et al.